# General-purpose photoelastic fiber optic accelerometer

**Wei Su**
MRL Inc.
5653 Stoneride Drive, Suite 102
Pleasanton, California 94588

**John A. Gilbert,** MEMBER SPIE
University of Alabama in Huntsville
Department of Mechanical and Aerospace Engineering
Huntsville, Alabama 35899
E-mail: jag@ebs330.eb.uah.edu

**Mark D. Morrissey**
**Yuehong Song**
University of Alabama in Huntsville
Consortium for Holography, Applied Mechanics and Photonics (CHAMP)
Huntsville, Alabama 35899

**Abstract.** This paper describes a general-purpose photoelastic fiber optic accelerometer having a sensitivity of 2 V/$g$ and a resolution of 2.5 m$g$ over a frequency range extending from 0 to 600 Hz. The unit has a linear amplitude range of 0 to 5$g$ and is sealed in an aluminum case having outside dimensions of 41 mm×35 mm×20 mm. It relies on a force transducer made from an optically birefringent material and measurements are made based on the principles of photoelasticity. A low-cost LED is employed as an incoherent light source; multimode optical fibers with a hard plastic cladding are used to transmit signals between the transducer and the conditioning electronics. 

Subject terms: acceleration measurement; transducer design; photoelasticity.

Paper 12046 received Apr. 12, 1996; accepted for publication Sep. 5, 1996.

## 1 Introduction

An accelerometer is an instrument used to measure the acceleration of a moving object. The most common types are piezoelectric, piezoresistive, and capacitive accelerometers.[1] However, none of these devices work well at high temperatures, and it is difficult to measure constant or steady-state acceleration with piezoelectric accelerometers because of the inherent problems associated with their operating principle. Many fiber optic accelerometers have also been developed.[2–8] In general, these units are very sensitive, weigh less than their electrical counterparts, and have a relatively high signal-to-noise ratio. The optical fibers also have the advantage that they are inert and immune to electromagnetic fields. The majority of the work performed in this area, however, has either focused on a specific application or been directed toward validation of a basic operating principle. As a result, fiber optic accelerometers lack the sophistication, reliability, and cost effectiveness enjoyed by their electrical counterparts. These obstacles currently limit the commercial production of fiber optic accelerometers and the widespread use of a potentially superior technology. The solution to this problem lies in the development of cost-effective and reliable units designed to meet a variety of different engineering applications.

This paper describes a general-purpose accelerometer which relies on a force transducer made from an optically birefringent material. A low-cost LED is employed as an incoherent light source, whereas multimode optical fibers with a hard plastic cladding are used to transmit signals between the transducer and the conditioning electronics.

## 2 Vibration Analysis and Transducer Design

The shape and arrangement of the parts contained within an accelerometer may be complicated; however, it is often possible to model the essential components by a relatively simple system consisting of masses, springs, and dampers. Figure 1, for example, shows the single-degree-of-freedom mechanical model with viscous damping used to characterize most force- and motion-measuring instruments. It is assumed that the instrument base is placed on, or fastened to, a machine or structure; the small mass of the base is usually neglected, since it becomes part of the mass of the structure to which it is fastened. The absolute displacements of the base and the mass are given by $x$ and $y$, respectively. The quantity

$$z = y - x \tag{1}$$

represents the displacement of the mass relative to the base.

The general equation of motion for the system is found by assuming that the motion of the base is sinusoidal with an angular frequency $\omega$ and an amplitude $X_0$, so that

$$x(t) = X_0 \sin \omega t. \tag{2}$$

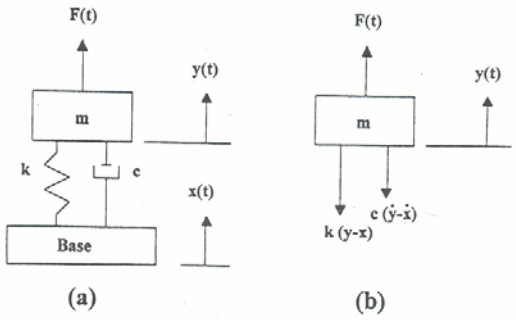


**Fig. 1** A single-degree-of-freedom model for a seismic acceleration transducer: (a) kinematic diagram, (b) free-body diagram.

  

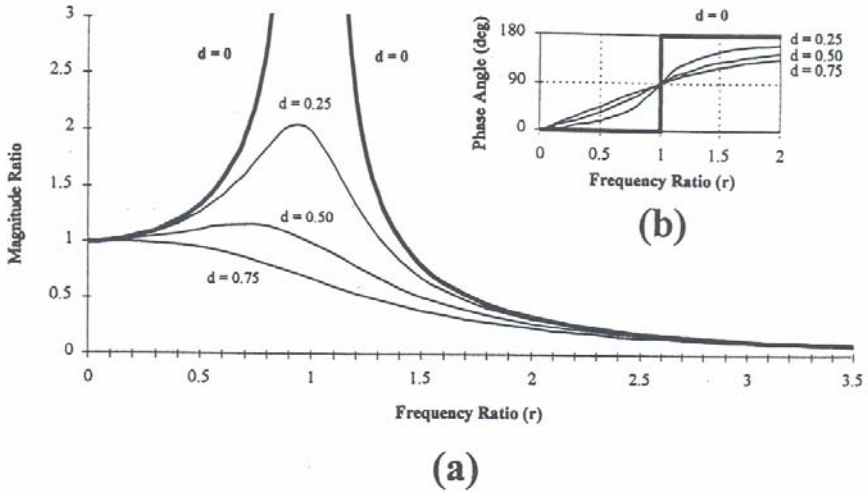


Fig. 2 The transfer function for a seismic acceleration transducer: (a) amplitude response, (b) phase response.

By applying Newton's second law to the free-body diagram shown in Fig. 1,

$$m\ddot{z}+c\dot{z}+kz=ma_0 \sin \omega t, \tag{3}$$

where

$$a_0=-\omega^2 X_0. \tag{4}$$

In Eqs. (2) and (3), $c$ is the damping coefficient, $k$ is the spring constant, and $a_0$ is the amplitude of the acceleration of the base in the direction of motion.

The term on the right-hand side of Eq. (3) represents a forcing condition dictated by the motion of the base, whereas the left-hand side defines the relative motion of the seismic mass contained within the instrument. The steady-state (particular) solution is[9]

$$z=\frac{-a_0 \sin(\omega t-\beta)}{\omega_n^2[(1-r^2)^2+(2rd)^2]^{1/2}} \tag{5}$$

where $r=\omega/\omega_n$ is the dimensionless frequency ratio and $d=c/2m\omega_n$ is the dimensionless damping factor. The natural frequency $\omega_n$ is a constant which depends upon the seismic mass and the stiffness of the spring via the relation $\omega_n=(k/m)^{1/2}$. The latter is associated with the complementary function that represents the transient solution obtained by setting the right-hand side of Eq. (3) equal to zero. The phase angle $\beta$ represents the degree to which the instrument response lags behind the motion which it measures; it is given by

$$\tan \beta=\frac{c\omega}{k-m\omega^2}=\frac{2rd}{1-r^2}. \tag{6}$$

The most important consideration for an accelerometer is how well the instrument is able to track the motion of the object. This can be studied by formulating a magnitude ratio defined as

$$\text{magnitude ratio}=\left|\frac{F_r/m}{a_0}\right|=\left|\frac{(kz)/m}{a_0}\right|$$

$$=\frac{1}{[(1-r^2)^2+(2rd)^2]^{1/2}}. \tag{7}$$

The influence of frequency upon forced amplitude can be studied by plotting the magnitude ratio against the dimensionless frequency ratio. Figure 2, for example, shows the transfer function corresponding to Eq. (5). For a given acceleration level $a_0$ and low to moderate damping ($d<0.5$), the elastic force measured in the spring, $F_r$, increases with the frequency ratio $r$. As a result, the acceleration transducer has different sensitivities for excitations at different frequencies; in the extreme case, $F_r$ may become infinite when the frequency ratio becomes unity; that is, when $\omega_n=\omega$, the system is at resonance.

The insert in the upper right-hand corner of Fig. 2 corresponds to Eq. (6); it shows that the phase angle between the base and the seismic mass also depends upon the frequency and can vary significantly from the desired value of zero. In general, these deviations in sensitivity and phase are undesirable, since they introduce distortions in the signal, making analysis difficult.

When the frequency ratio is small, however, it is observed that the magnitude ratio is approximately equal to unity regardless of the amount of damping. For this case, the phase angle $\beta$ also approaches zero. Specifically, for $d=0$, illustrated with heavy black lines on Fig. 2 and the most critical case for the onset of resonance, and $r<0.2$, the magnitude ratio and phase angle deviate by less than 5% from unity and zero, respectively. These deviations and the associated errors are considered allowable from a practical

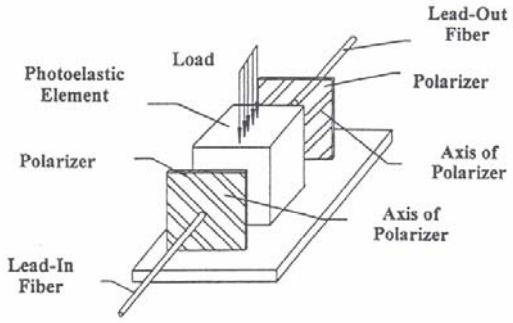


Fig. 3 A photoelastic fiber optic force transducer.

standpoint; consequently, a seismic acceleration transducer incorporates as little damping as possible and is designed to function at frequencies below 20% of its natural frequency. When both $r$ and $d$ are small, Eq. (5) reduces to

$$z = -\frac{1}{\omega_n^2} a_0 \sin \omega t = -\frac{ma_0}{k} \sin \omega t. \tag{8}$$

In this case, the force in the spring, $F_r = kz$, is

$$F_r = -ma_0 \sin \omega t. \tag{9}$$

Equation (9) shows that the force is directly proportional to the acceleration; $F_r$ can be measured using a photoelastic fiber optic force transducer.

## 3 Photoelastic Fiber Optic Force Transducer

Many noncrystalline transparent materials which are ordinarily optically isotropic become anisotropic and display optical characteristics similar to crystals when they are stressed. This phenomenon, known as temporary birefringence, forms the basis for the science of photoelasticity.[10]

Figure 3 shows a schematic diagram of a photoelastic fiber-optic force transducer recently reported by Su et al.[11] It consists of a photoelastic cube, two crossed polarizers, and two optical fibers. A stress concentration is produced by the applied load and the quadrature condition is achieved by preloading the transducer. Since the stress distribution directly below the load is uniaxial, the isoclinics in this region are eliminated when the polarizers are oriented at 45 deg with respect to the loading. In this case, the light intensity modulation, $\Delta I$, produced by a variation in the principal stress difference, $\Delta\sigma_d$, is[11]

$$\frac{\Delta I / I_0}{\Delta \sigma_d} = \frac{\pi t_s}{f_\sigma}, \tag{10}$$

where $I_0$ is the intensity of the incident light, $t_s$ is the thickness of the sensing element, and $f_\sigma$ is the material fringe value. When the photoelastic material remains within the elastic region, $\Delta\sigma_d$ is proportional to the force exerted on the transducer.

Figure 4 shows a typical fringe pattern produced when a load $P$ is applied to the sensing element. The theory of

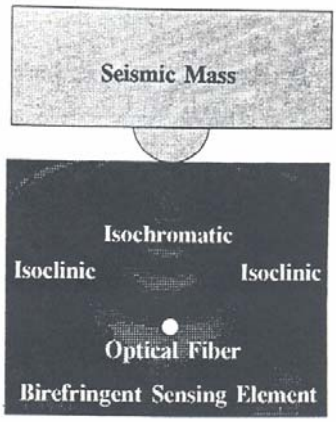


Fig. 4 The combined isochromatic and isoclinic pattern produced by applying a concentrated load to a semi-infinite plate. The pattern was recorded using a dark-field plane polariscope with crossed polarizers oriented at 45 deg with respect to the loading. The optical fiber is located so that the quadrature condition is achieved.

elasticity can be applied to determine the stresses in polar coordinates for points located directly beneath the load. In this case, Eq. (10) becomes

$$\frac{\Delta I / I_0}{\Delta P} = \frac{2}{f_\sigma R}, \tag{11}$$

where $\Delta I$ is the light intensity modulation for a given load increment $\Delta P$, and $R$ is the radial distance measured from the free surface to the point in question.

Equation (11) indicates that the sensitivity of the photoelastic fiber optic force transducer can be adjusted simply by changing the point at which the isochromatic pattern is sampled. This can be accomplished physically by adjusting the positions of the optical fibers that transmit light to and from the sensing element. The advantage of this approach is that the gain of the transducer can be adjusted mechanically without introducing noise.

## 4 Photoelastic Fiber Optic Accelerometer

The force transducer, illustrated in Fig. 3, was incorporated into the accelerometer design depicted in Fig. 5. The mass

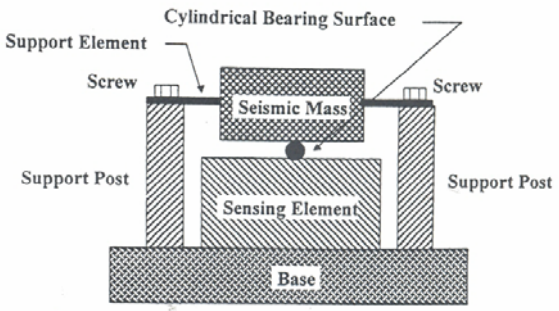


Fig. 5 A schematic representation of the photoelastic fiber optic accelerometer.

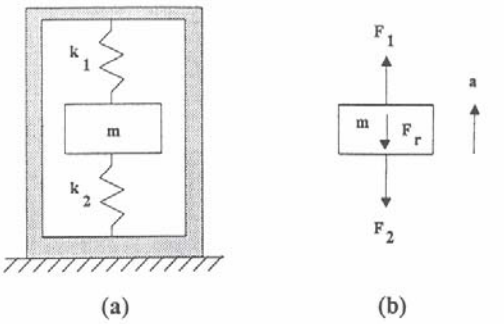


Fig. 6 A dual-spring, single-degree-of-freedom system: (a) kinetic diagram, (b) free-body diagram.

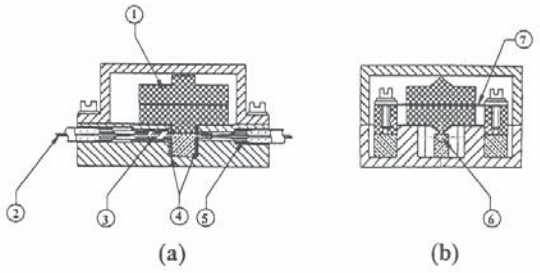


Fig. 7 An assembly drawing of the general-purpose photoelastic fiber optic accelerometer: (a) front view; (b) side view. 1, seismic mass; 2, optical fiber; 3, GRIN lens; 4, linear polarizer; 5, fiber optic ferrule; 6, photoelastic sensing element; 7, support element.

is supported by two spring elements, which are tilted to preload the sensing element. The symmetrical geometry minimizes transverse sensitivity. The line contact between the seismic mass and the sensing element produces the desired stress concentration, while the symmetric distribution of mass with respect to the springs reduces the rotation (and the corresponding response) that results from transverse acceleration.

Since the sensing element is compliant and deforms in response to the applied load, it also acts as a spring. Figure 6 shows the equivalent dynamic model for the accelerometer. The model consists of two springs acting on opposite sides of a mass; the first spring has a spring constant $k_1$ equivalent to the composite stiffness of the two elements used to suspend the seismic mass above the sensing element, while the second spring has a spring constant $k_2$ equivalent to the stiffness of the photoelastic sensing element itself. By the nature of the design, damping is negligible.

The equation of motion for this model is given by Eq. (3) with $d=0$ and $k=k_1+k_2$. Consequently, the natural frequency of the transducer is

$$\omega_n=\left(\frac{k_1+k_2}{m}\right)^{1/2}. \tag{12}$$

Equation (12) shows that, for a given photoelastic element, the natural frequency of the transducer can be adjusted either by changing the size of the seismic mass or by modifying the stiffness of the beam.

The force between the seismic mass and the base, expressed as $F_r$ in Eq. (9), is the sum of the forces exerted by the two springs, while the inertia force acting on the sensing element is

$$F_2=F_r\frac{k_2}{k_1+k_2}. \tag{13}$$

Equation (13) indicates that the sensitivity of the accelerometer increases when weaker elements, having a smaller stiffness, are used to support the mass (that is, more inertia force is transferred to the sensing element). In this case, the required natural frequency (5 times the highest frequency to be measured) can be achieved by choosing a suitable seismic mass $m$ based on the stronger stiffness of the sensing element, $k_2$.

For the unit to function properly, the preload must be much larger than the inertia force imposed on the accelerometer during maximum acceleration; the preload must also be adjusted to ensure that the transducer is working at the quadrature condition. It should be noted that a weaker supporting elements make it easier to accurately adjust the preload, since the preload is proportional to the product of the deflection and the stiffness of the elements.

The range over which the sensitivity to acceleration remains constant to within a certain level, typically taken as a few percent, is defined as the linear amplitude range. The linear amplitude range of an accelerometer depends on the inherent characteristics of all transducers in the measurement system. For example, nonlinearities can be introduced in the force transducer by the nonlinear behavior of the spring which may occur for a large displacement. Because every transducer is only linear over a certain range, specifying the latter is of critical importance to the designer. The lower limit of the linear amplitude range depends upon the noise level of the overall system, whereas the upper limit is affected by the fragility of the accelerometer as a whole, and by the nonlinear response of the transducers and/or the signal conditioner. A comprehensive knowledge of mechanics, physics, and electro-optics is required to meet design specifications.

## 5 Prototype System

A general-purpose photoelastic fiber-optic accelerometer was designed to measure frequencies that ranged between 0 and 600 Hz. The equivalent stiffnesses of the support elements and the sensing element were computed by using beam deflection theory and by solving the Hertzian contact problem, respectively. The natural frequency and the sensitivity of the accelerometer were achieved by choosing an appropriate mass and sensing material, respectively. The unit was designed to have a linear amplitude range between 0 and $5g$.

Figure 7 shows the acceleration transducer, which is sealed in an aluminum case having outside dimensions of 41 mm×35 mm×20 mm. In order to achieve high sensitivity, the sensing element is made of a photoelastic material, PSM-1, having a stress optical coefficient of $7.8\times10^{-5}$

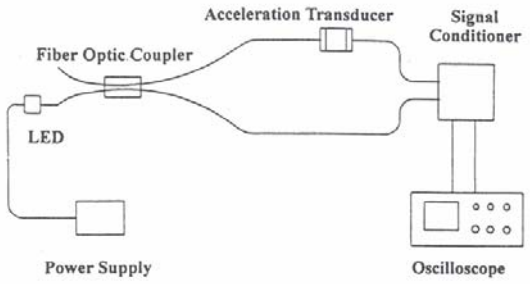


Fig. 8 A photoelastic fiber optic accelerometer measurement system.

$mm^2/N$. The element is placed between two crossed linear polarizers and loaded using a 20-g seismic mass. The latter is made from copper to reduce the overall dimensions. The support elements are made from stainless-steel shim stock, while most of the surrounding structure is constructed using an aluminum alloy. The radius of the cylindrical surface at the point of contact is 0.5 mm, and a preload of 1.0 N is applied to the sensing element. Optical access to the transducer is provided through two 200-$\mu$m-diam multimode optical fibers. Fiber optic ferrules, used to hold the fibers in place, simplify the alignment procedure. A 0.5-pitch GRIN lens is used to collimate the light and increase the optical coupling efficiency.

## 6 Calibration

Following the assembly of the accelerometer, tests were conducted to experimentally evaluate its performance relative to the design specifications. The experimental set up, shown in Fig. 8, relies on an incoherent light source having a peak emission wavelength of 0.82 $\mu$m; at this wavelength, the material fringe value of the sensing element is 10.5 kPa/(fringe/m). A reference leg is included in the system to correct for the intensity modulation that may occur in the light source. A signal conditioner, consisting of a photodetector, a differential amplifier, and a low-pass filter, was custom-designed and fabricated to facilitate the measurement. The photodetector consists of a dual-channel photodiode–operational-amplifier combination; a digital oscilloscope is used to acquire, display, and process the signal from the signal conditioner. The digitized signal can be sent to a computer using an RS-232 line or a GPIB interface.

The sensitivity of the general-purpose accelerometer was so high that it was calculated at zero frequency (constant acceleration) using local gravitational attraction and the absolute calibration method. In this method, the unit is fixed on a rotating stage and the output of the accelerometer is recorded with respect to the angle of rotation. The output is zeroed when the accelerometer is mounted in the normal position, that is, with the sensitivity axis in the vertical direction. In this position, the seismic mass is subjected to $1g$. As the unit is rotated, the projection of the acceleration (gravity) vector in the sensitivity direction decreases, resulting in a decrease in output. When the accelerometer is turned upside down, a net change of $2g$ takes place. Figure

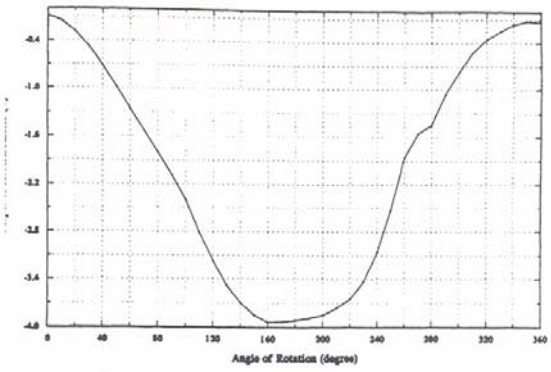


Fig. 9 The response of the general-purpose photoelastic fiber optic accelerometer obtained by the absolute calibration method.

9 shows the test results obtained from the absolute calibration method. The peak-to-peak amplitude corresponds to$2g$; the slight deviation from the anticipated sinusoidal shape is attributed to the microbending effects which occur in the optical fibers during rotation. The sensitivity of the accelerometer was adjusted to 2.0 V/$g$ by changing the gain of the signal conditioner.

The frequency response of the accelerometer was determined using an electrodynamic shaker. The general-purpose photoelastic fiber optic accelerometer was bonded to a standard piezoelectric accelerometer; the combination was mounted on top of the shaker with the sensitivity axes of the accelerometers aligned with the direction of motion. The shaker was driven with sinusoidal inputs having frequencies ranging from zero to 10 kHz. The outputs from the accelerometers were recorded using a dual-trace oscilloscope. The transfer function for the general-purpose photoelastic fiber optic accelerometer was calculated from these data and is plotted in Fig. 10. The figure shows that the natural frequency of the accelerometer is approximately 3.5 kHz; this value is within 3% of the anticipated value obtained from numerical analysis. The

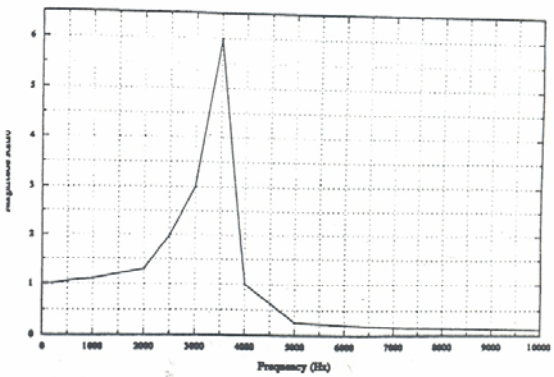


Fig. 10 The transfer function for the general-purpose photoelastic fiber optic accelerometer.

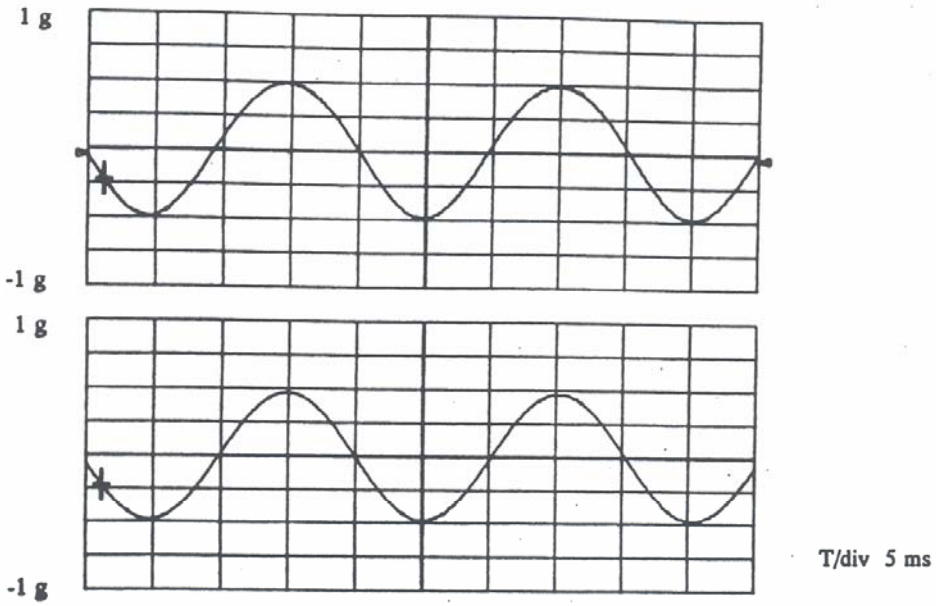


**Fig. 11** The dynamic response at 50 Hz of two different accelerometers. Upper trace: photoelastic fiber optic accelerometer; lower trace: piezoelectric accelerometer.

sensitivity of the general-purpose accelerometer is nearly constant below the maximum operating frequency of 600 Hz.

The outputs from the two accelerometers were identical over the frequency range extending from 10 through 600 Hz; Fig. 11, for example, shows the outputs for a frequency of 50 Hz. Below 10 Hz, the output from the piezoelectric accelerometer quickly decreases, whereas the output from the photoelastic fiber optic accelerometer remains constant.

Other tests showed that the transverse sensitivity is less than 1% and that the photoelastic fiber optic accelerometer is basically insensitive to lead-in and leadout provided that the fibers are not subjected to extremely large vibration amplitudes. The temperature sensitivity was measured at $0.0224g$/°C. The noise level is approximately 5 mV, making the resolution 2.5 $mg$.

## 7 Conclusion

This paper has outlined the design considerations and calibration procedures used to develop a general-purpose photoelastic fiber optic accelerometer. The prototype has a sensitivity of 2 V/$g$ over a frequency range extending from 0 to 600 Hz and a linear amplitude range of 0 to 5$g$. Since the noise level is approximately 5 mV, the resolution is 2.5 $mg$. These performance levels are comparable to those associated with the best electrical accelerometers on the market, but, unlike its electronic counterparts, the photoelastic fiber optic accelerometer can be used at elevated temperatures and can detect signals down to dc. With its compact size, high reliability, high performance, and simplicity, the photoelastic fiber optic accelerometer offers significantly greater market potential than all other optical accelerometers previously reported in the literature.

## Nomenclature

| | |
|---|---|
| $a_0$ | amplitude of the acceleration of the transducer base |
| $c$ | damping coefficient |
| $d$ | dimensionless damping factor |
| $f_\sigma$ | material fringe value |
| $g$ | gravity |
| $k$, $k_1$, $k_2$ | spring constant |
| $m$ | mass |
| $r$ | dimensionless frequency ratio |
| $t$ | time |
| $t_s$ | thickness |
| $x$ | displacement of the transducer base |
| $y$ | displacement of the mass |
| $z$ | relative displacement between the mass and the transducer base |
| $z_0$ | static displacement for a constant acceleration |
| $F_r$, $F_2$ | spring force |
| $I_0$ | intensity |
| $R$ | distance between applied load and free surface |
| $X_0$ | amplitude of the motion of the base |

| | |
|---|---|
| $\beta$ | phase angle |
| $\Delta I$ | modulation in intensity |
| $\Delta P$ | modulation in load |
| $\Delta\sigma_d$ | modulation in principal stress difference |
| $\lambda$ | wavelength |
| $\omega$ | angular frequency |
| $\omega_n$ | natural frequency. |

## Acknowledgment

Support for the project was provided by the Consortium for Holography, Applied Mechanics and Photonics at the University of Alabama in Huntsville.

## References

1. A. Karolys and G. Pender, "Present and future of acceleration and pressure measurement systems," in *Proc. 40th Annual Earthmoving Industry Conference*, Peoria, IL, Apr. 11–13 (1989).
2. A. B. Tventen and A. Dandridge, "Fiber optic accelerometer," *Electron. Lett.* **16**, 854–856 (1980).
3. A. D. Kersey, D. A. Jackson, and M. Corke "High-sensitivity fiber-optic accelerometer," *Electron. Lett.* **18**(13), 559–561 (1982).
4. D. L. Gardner, T. Hofler, and S. R. Baker, "A fiber-optic interferometric seismometer," *J. Lightwave Technol.* **LT-5**, 953–959 (1987).
5. M. R. Layton, B. A. Danver, J. D. Lastofa, and D. P. Bevan, "A practical fiber optic accelerometer," in *Fiber Optic and Laser Sensors V. Proc. SPIE* **838**, 279–284 (1987).
6. D. A. Brown and S. Garrett, "An interferometric fiber optic accelerometer," in *Fiber Optic and Laser Sensors VIII, Proc. SPIE* **1367**, 282–288 (1990).
7. J. B. Freal, C. J. Zarobila, and C. M. Davis, "A microbended horizontal accelerometer for borehole deployment," *J. Lightwave Technol.* **LT-5**, 993–996 (1987).
8. G. Conforti, M. Brenci, and A. Mencaglia, "Optical fiber sensor for vibration monitoring in high power electrical plants," in *Fiber Optic Sensors III, Proc. SPIE* **1011**, 116–119 (1988).
9. R. K. Vierck, *Vibration Analysis*, International Textbook Co., 1969.
10. M. M. Frocht, *Photoelasticity*, Vol. I, Wiley, 1948.
11. W. Su, J. A. Gilbert, and C. Katsinis, "A photoelastic fiber optical strain gage," *J. Exp. Mech.* **35**(1), 71–76 (1995).

Biographies and photographs of the authors not available.